Submicron focusing of hard X-rays with reflecting surfaces at the ESRF

Olivier Hignette*, Gérard Rostaing, Peter Cloetens, Amparo Rommeveaux,
Wolfgang Ludwig, Andreas Freund
European Synchrotron Radiation Facility, Grenoble, France

ABSTRACT

We describe Kirkpatrick-Baez (KB) reflecting mirror systems that have been developed at the European Synchrotron Radiation Facility (ESRF). They are intended to be used mainly in the hard x-ray domain from 10 KeV to 30 KeV for microfluorescence, microdiffraction and projection microscopy applications. At 19 KeV a full width at half maximum (FWHM) spot size of 200X600 nanometers has been measured and with an estimated irradiance gain of $3.5x10^5$. The alignment and bending processes of the system are automated based on the wavefront information obtained by sequentially scanning slits and reading a position-sensitive device located in the focal plane. The sub-microradian sensitivity of this method allows us to predict the spot size and to provide a metrology map of the surfaces for future improvements of the performances. A novel device based on specular reflection by a micromachined platinum mirror has been used to determine the spot size with an equivalent slit size of less than 100 nanometers.
Projection phase images of submicron structures are presented which clearly show both the high potential and also the present limitations of the system. First microfluorescence images obtained at 20.5 KeV are shown. Finally, a roadmap towards diffraction-limited performance with metal and multilayer surfaces is presented.
Keywords: X-ray mirrors, microfocusing, Kirkpatrick-Baez geometry, holotomography, microfluorescence, microdiffraction.

1. INTRODUCTION

Microfocusing techniques are very important for applications of x-ray scattering and absorption to many research areas such as physics and chemistry, materials and life sciences, environmental research, high-pressure based research, etc. Almost as many methods to obtain small, very even sub-micron spot sizes have been developed, in particular for synchrotron x-ray instrumentation. Amongst them are Fresnel zone plates, curved crystals, mirrors and multilayers, tapered capillaries, and more recently refractive lenses and waveguides. They all have specific advantages and disadvantages depending on the experiments to be performed. Some of them are the subject of papers of this conference, others have been published in earlier SPIE conference proceedings or proceedings of synchrotron radiation instrumentation conferences. The aim of this paper is not to compare the various techniques, but to report on the most recent progress achieved at the ESRF with a special combination of orthogonal mirrors called Kirkpatrick-Baez optics. This very powerful optical device and its performances, based on single and multilayer mirrors, have been described in several papers; the most recent ones are by Underwood *et al.*[1] Padmore *et al.*[2], and Eng *et al.*[3] the latter achieving a spot size as small as 800 x 850 nm^2 at an x-ray energy of 10 KeV with a gain factor of 10^5. We have tried to still increase the performance of this technique by improving the substrate quality and by more accurate bending of initially flat substrates.

2. DESIGN PRINCIPLES

Once we have chosen to use specularly reflecting surfaces for the Kirkpatrick-Baez crossed mirror geometry, the design optimization starts by analyzing the constraints of a given application and possible trade-offs with existing technology.
A low-beta undulator source at the ESRF has a typical horizontal source size S_h of 125 microns (FWHM) that is about 5 times larger than its vertical size, S_v. For high-beta sections S_h = 800 microns and the ratio S_h/S_v is as high as 40. The horizontal source has to be demagnified as much as allowed by the effective working distance, q_h. Therefore, the first limitation of producing a sub-micron spot size $F_h = S_h/M_h$ originates from the horizontal source size, the source-to-optics

* Hignette@esrf.fr; phone 033476882747; fax 033476882545; optics group ESRF; BP220 38240 Grenoble CEDEX FRANCE

X-Ray Micro- and Nano-Focusing: Applications and Techniques II, Ian McNulty, Editor,
Proceedings of SPIE Vol. 4499 (2001) © 2001 SPIE · 0277-786X/01/$15.00

and the optics-to-sample distance p_h and q_h, respectively. $M_h = p_h/q_h$ is the horizontal magnification. Then the vertically focusing mirror contributes to the spot size F_v in the vertical direction essentially through its figure error and this contribution is proportional to the distance q_v. The length of the mirrors is governed by the size of the synchrotron beam that should be accepted by the optics, A_h and A_v, respectively, and by the glancing angle, θ. Three generic designs have been produced to allow for some flexibility, with mirror lengths of 92 mm and 170 mm. Fig 1 shows the KB-I model with two 170 mm long mirrors and Fig 2 shows the KB-II model with two 92 mm long mirrors. The angular and linear adjustments are achieved by combining two rotations. Four microjacks and flexure pivots are used to combine compactness and angular stability. Four picomotors provide submicroradian-bending sensitivity. The mirrors must be shaped according to the required working distance and the energy range determines the choice of the coating. The required stigmatic surfaces, elliptical in meridional direction and flat in sagital direction, are obtained by applying two different moments at the ends of flat polished substrates that have constant thickness, but linear width variation. Several similar techniques are described [1,5] in the literature. Our bending technology, based on flexural hinges, was described by Zhang et al [4]

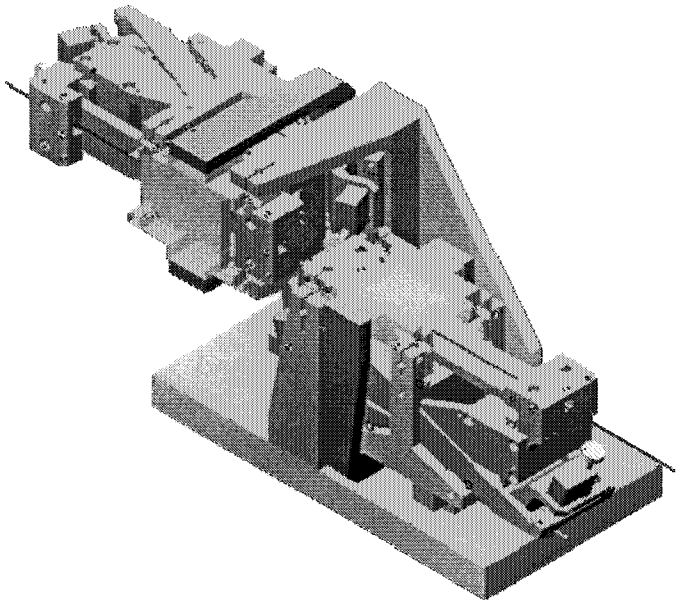

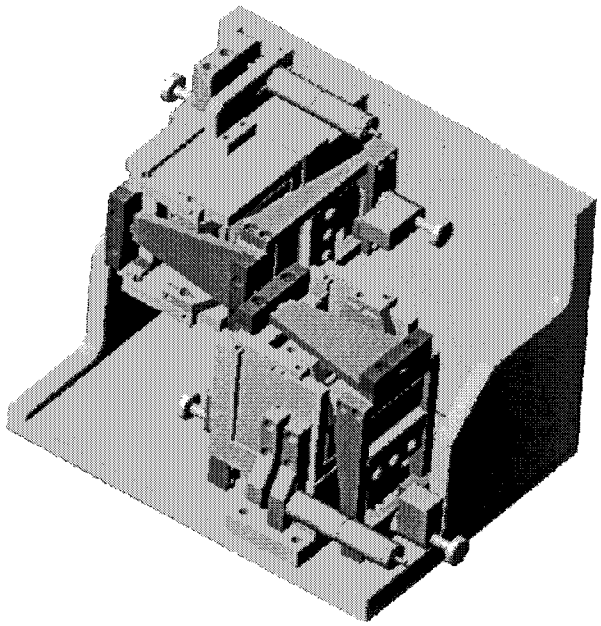

Fig.1 KB I Kirkpatrick - Baez system with two 170 mm mirrors Fig.2 KBII system with two 92 mm shaped substrates

3. STIGMATIC FIGURING APPROXIMATION:

The mirror stigmatic figure needed to get a minimum spot size is an ellipse whose shape z (x) can be approximated as [6]:
$z(x) = \alpha x^2 \left(1 + \beta x + \gamma x^2\right)$, Where x is centered on the pole of the mirror

With $\alpha = \frac{\sin\theta}{4p}\left(1+\frac{p}{q}\right)$, $\beta = \frac{\cos\theta}{2p}\left(\frac{p}{q}-1\right)$, $\gamma = \frac{1}{4pq} + \frac{5\cos^2\theta}{16p^2}\left(1-\frac{p}{q}\right)^2$ (1)

and p is the source – mirror center distance, q is the mirror sample distance (focal length) and θ is the incidence angle.
The third order terms of the equation can be matched with a constant width mirror bent with two different moments applied at both its ends [4], but the fourth order requires to vary the its moment of inertia along its meridional axis.
In order to machine the mirror with a simple manufacturing process, we have chosen a linear width variation W (x) designed according to $W_1(x) = W_0(1 + 2\psi x)$, where ψ is the half angle of the resulting trapezoidal shaped mirror and W_0 the width at the center of the mirror. Combining the equation (28), (29), (30) of reference [6] leads to the very simple result:

$$\psi = \frac{W_0\,\gamma}{\beta} \quad (2)$$

This result is in very good agreement with the more elaborated non-linear optimization method described by P.Eng [3]. Its main implication is that, within the limits of validity of the approximations and for small angles where cos θ is close to one, the width does not depend on the incidence angle but only on the source and sample distances.

In order to evaluate the degradation of the performance of the system with respect to the stigmatic reflecting surface (ellipse), we assume a nearly perfect ellipse would be obtained with a quadratic width variation

$$W_2(x) = W_0\left(1 + 2\psi\, x + \zeta\, x^2\right) \quad (3)$$

The difference between $W_1\ and\ W_2$ leads to an error on γ, which is $\Delta\gamma = \left(\frac{\gamma\ W_0}{2\psi\ L} + \frac{\beta}{2\,L}\right)$ where L is the length of the mirror. The error on the shape of the mirror is therefore $\Delta z = \frac{\alpha\, x^4}{2L}\left(\frac{\gamma W_0}{\psi} + \beta\right)$. This error is added to the perfect elliptical shape and the resulting surface used by a specifically developed ray-tracing program (KB_Ray). The resulting spot broadening is immediately obtained. In all design cases we have dealt with so far, including incidence angles smaller than 15 milliradian, the quadratic width variation was found unnecessary.

The KB_Ray program is performing a sequential monodimensionnal ray-tracing by simulating the undulator or bending magnet source as an angular and spatial Gaussian distribution. The focal plane positions of the rays, properly weighted by ray intensity, are histogrammed to get the spot size prediction with a high degree of precision. All the rays launched through the system contribute to the histogram, an advantage over Monte Carlo type programs. The consistency of the results of KB_Ray has been tested positively with respect to SHADOW. This incoherent ray-tracing approach is becoming limited as the technology evolves towards systems partially preserving the coherence of the source, and true Fresnel propagation is being introduced in the program to analyze those systems. The influence of a real mirror surface as measured by the Long trace profiler (LTP) or by an X ray wavefront in situ analysis [8] is predicted with KB_Ray by importing the proper files formats.

4. SUBSTRATE WIDTH AND THICKNESS TOLERANCES

4.1 Substrate thickness tolerance in the meridional direction:

It is assumed that the 2 moments bending mechanism can perfectly correct a third order polynomial shape. The criteria of quality is therefore the rms slope error of the surface detrended by a second order polynomial.

A constant section beam presents a local curvature C (x) proportional to the moment M (x) [4]

$$C(x) = \frac{M(x)}{E\,W(x)\,t^3(x)} \quad (4)$$

Where W is the width and t the thickness of the beam, E the Young Modulus .The slope Δ(x) can be expressed as $\Delta(x) = \int C(x)dx = \Delta_0 + \int \frac{\partial C(x)}{\partial t}\delta\, t(x)\, dx$. The thickness deviates from its nominal value t_0 by a small amount δt (x) along the mirror, the mean curvature being C_0. It can be shown that:

$$\Delta(x) = \Delta_0 - \frac{3C_0}{t_0}\int_0^x \delta t(x)dx \quad (5)$$

A possible wedge between upper and lower surface translates into a second order polynomial slope error that can be compensated by two adequate moments. This implies that the first significant term is the curvature of the back surface, if we assume the front surface to be perfectly flat. Higher order terms can be taken into account, but are less important in

practice. The shape of the back surface can be expressed as $\delta t = \frac{C_1 x_c^2}{2}$, where the origin of C_x is at the center of the mirror. The slope is then

$\Delta(x_c) = -\frac{3C_0 C_1}{2t_0}\left(\frac{x_c^3}{3}\right)$, With L representing the length of the mirror.

The variance of the slope error is $(\delta\Delta_{rms})^2 = \left(\frac{3C_0 C_1}{2t_0}\right)^2 \frac{2}{L}\int_0^{L/2}\left(\frac{x_c^{\,3}}{3}\right)^2 dx_c$, and its standard deviation

$$\delta\Delta_{rms} = \frac{C_0 C_1 L^3}{16\sqrt{7}\, t_0} \quad (6)$$

The radius R1 of the of the back surface has to be larger than $R_1 = \frac{0.023L^3}{\delta\Delta_{rms}\, t_0 R_0}$

As an example, for the system located on the beamline ID19, described in this paper, the horizontal mirror radius must be larger than 100m for a slope error tolerance of 0.2 μrd rms, or a parallelism error of 4 micron (13 fringes for opticians). This is already a non-trivial job for thin mirrors. For the vertical one, the radius has to be larger than 160 m. For multilayers or lower energy systems where the incidence angles and curvatures are larger, this becomes a major mirror manufacturing issue.

4.2 Substrate thickness tolerance in the sagital direction

The holding mechanisms at both ends of the mirror have to be designed in such a way as to compensate for any wedge, but after all clamping mechanical parts have been grinded and polished to optical precision (less than one fringe). The remaining sagital curvature and non flatness will result in uncontrolled stresses which in turn induce twisting and non linear surface effects. As evidenced on control interferograms, polishing the clamping parts has resulted in dramatic improvements of the mirror shape.

4.3 Width tolerance

A similar analysis leads to:

$\Delta(x) = \Delta_0 - \frac{C_0}{W_0}\int_0^x \delta W(x)dx$ (7) . Here again, a small linear error on the width, equivalent to modifying the trapezoid shape angle, translates into a second order polynomial slope error that is easily compensated by adjusting the two moments. Because the width is typically 10 times larger than the thickness and because of the factor of 3 between equations (5) and (7), the width tolerances as obtained from the grinding operation are easier to control .

5. OTHER LIMITING FACTORS

5.1 Substrate polishing non flatness

Any deviation of the flat substrate, before bending, from a third order polynomial shape cannot be compensated by the active bending mechanism. It would be beneficial to choose a thick substrate for ease of polishing, but then the forces to be applied become large and the radius stability is a concern. The best quality substrates we obtain commercially present slope error standard deviations (second order polynomial detrended) of Δ=0.3 microradian rms. This contributes to in the spot size full width half maximum (FWHM) as [6] FWHM = 4.7 Δ q

5.2 Clamping induced errors

Any method of attachment of the substrates to the bending mechanism produces non-uniform stresses, which induce twist and a degradation of the meridional slope error. One major challenge is that a relative radius drift smaller than 10^{-3} can only be tolerated after a change in curvature (for example imposed by a large energy tuning).

This implies a strong attachment of the mirror to the substrate. A continuous program of development, comparing clamping and gluing methods is under progress at the ESRF .The present designs are referencing the front surface for 170 mm mirrors and the back surface for 92 mm type. They are not affecting in a measurable way the slope error of present state of the art mirrors provided surfaces in contact are of comparable flatness (less than one fringe).

5.3 Bending errors

When the sensitivity of the actuators and a proper feedback system is used [9],the in situ measured second order polynomial slope error becomes less than 0.1 microradian rms. It can be can be considered as negligible.

5.4 Vibrations, angle stability and radius drift

A vibration of peak to valley amplitude A broadens the spot size by roughly a factor of: 2 A q. In order not to limit the vertical spot size, this amplitude must be of the same order as the rms slope error of the mirror, i.e. less than 0.3 microradian. Precise measurements of vibration levels have been undertaken, showing that this is a realistic goal in our facility with careful structural design, but this might become a major limiting factor for future (diffraction limited) devices. The relative variation of the focal length induces a linear broadening of the spot size Δs, which is proportional to the useful aperture $L\,\theta$ and to the angle of incidence drift $\Delta\,\theta$. This effect can also be produced by a mirror radius drift $\Delta\,R$ according to the linear relationships:

$$R \cong \frac{2q}{\theta} \qquad \frac{\Delta s}{L\theta} = \frac{\Delta\theta}{\theta} = \frac{\Delta R}{R}$$

These relative quantities are of the order of 10^{-3} in our submicron applications, placing tight error budgets on radius and incidence angle drifts .

6. SYSTEM OPTIMIZED FOR PROJECTION IMAGING ON ID 19

6.1 Design goals:

Phase imaging and holotomography [7] applications on the ID19 imaging devoted beamline require a high energy (around 20 KeV) for samples investigated in transmission. To get sufficient acceptance, the mirrors are coated with Platinum and used at θ= 3 mrd incidence angle. Experiments have been run at 19 KeV and 20.5 KeV. A minimum working distance of 50 mm has been kept, since it is required by most other applications to allow for some sample diffractometer space. This leads to focal distances q_H=96 mm and q_V = 280 mm. With a beamline length p= 146 meters, the demagnification factors of the source are M_H= 1460 and M_V= 517 in horizontal and vertical directions. The demagnified FWHM source sizes in the focal plane are 92 nanometers and 48 nm. The length of the beamline, p= 146 meters, leads to angular source sizes, as seen

from the mirrors, of $\Omega_V = 0.17\ \mu rd \ \ and \ \ \Omega_H = 0.92\ \mu rd$ in the vertical and horizontal directions respectively. From geometrical considerations only, the mirror figuring slope errors standard deviation ($\delta\Delta v_{rms} \ and \ \delta\Delta h_{rms}$) should be less than a fourth of these values not to limit the performance of the system. This approximation is not true anymore in the vertical direction since the coherence length $l_{coh} = \frac{\lambda}{2\Omega_v}$ is equal to 200μm or nearly the full 280μm acceptance. The proper criteria for a coherent system are not anymore slope but shape error.

According to the Marechal's criteria [8], $\sigma = \frac{\lambda}{27\sin\theta}$, a mirror with a standard deviation figure error σ =0.8 nanometer will lead to diffraction limited performance at 19 KeV and 3 mrd incidence, independently of the source size. The smallest dimension achievable in the vertical direction with such a quality would be governed by the diffraction of the 280 μm slit used and the corresponding numerical aperture Φ according to $FWHM_V = 0.45\ \lambda/\sin\Phi$ =65 nanometers (sinc function of a rectangular aperture). This means that the demagnified source size limit (48 nm) cannot be reached with such a system. in the vertical direction, even with perfect mirrors.

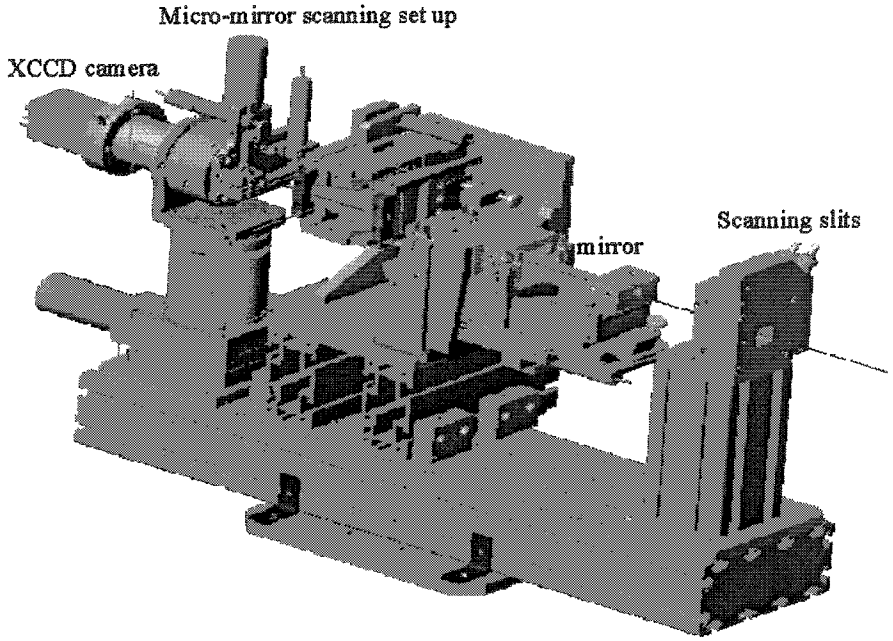

Fig.3 ID19 set up (KB III), showing the scanning slits used for automated alignment and bending. The six degrees of freedom scanning set up holding the XCCD camera and the micro-mirror, with 30 nm increments movements, has also been used for building the microfluorescence image.

With the present available technology, the spot size is limited by the mirror quality in both directions, consequently the incoherent approximation consisting of ray tracing independent rays through the system to predict its behavior is still valid. The projection microscopy application ideally requires the same illumination angle in both directions. The vertically focusing mirror, further away from the sample, has to be larger than the horizontally focusing one, leading to a compound KBIII system with 92 + 170 mm long mirrors. Both substrates have been provided by Wave Precision (Moorpark, CA), the 92 mm long one with an optimum trapezoidal shape, and the vertical focusing one with rectangular shape.

6.3 ID 19 Experiment

The experimental set up shown in Fig.3 was installed on a beamline diffractometer in the experimental hutch. The energy is selected by a Si 111 monochromator. Four motor slits are used to define the beam and are scanned for bending optimization [9]. The KB system is adjusted with 8 motors and the sample holder with 5 motors. A XCCD camera is used for alignment and wavefront analysis then dismounted to allow a micromirror to be scanned in the focal plane for spot size measurement. This micromirror technique has been introduced to improve the precision of measurement obtained with the more classical knife edge method. The derivative procedure needed with the latter method requires that the displacement increments be known with an extreme accuracy when they become smaller than 50 nanometers and the quality of the fluorescence knife-edge is difficult to control. We are instead using a narrow (25 and 50 microns width) stripe of platinum on a supersmooth (roughness 0.8-angstrom rms) silicon mirror. When aligned at 2.8 mrd grazing angle, the full angular acceptance of the KB at 19 KeV is reflected at less than 5 % by the silicon region and more than 75 % by the platinum region, acting as a slit of an equivalent width of 70 and 140 nm respectively. These micromirrors have been etched by an ion beam-milling machine [8], recently developed in the ESRF optics group. The mask is a 50 μm or 25 μm tungsten wire (Goodfellow).

6.4 Prealignment and alignment

The mirror curvatures are set up in the optics metrology lab with the LTP using a linear optimization procedure [8].
The whole set up was prealigned in the optics lab with respect to gravity and autocollimated with respect to a gravity aligned laser. The mirror incidences are set with respect to the laser beam to 3 mrd; slits and camera are aligned with the laser. The set up is then installed on the beamline and adjusted with respect to a laser aligned with respect to the X-ray beam. The estimated precision of the procedure is +/- 0.3milliradian and +/- 0.5 mm. When the shutter was opened, the reflected spot was on the center of the camera with a spot size of 15X18 microns. This operation is irrelevant for a

permanent set up but important when only a few beamtime shifts are granted for test. It is also needed for applying our standard camera based autoalignment procedures.

6.5 Bending and mirror metrology with wavefront analysis

The optimization of the wavefront by bending the mirrors is obtained with a linear least square method which has been used at the ESRF for more than 4 years [9]. It consists in creating a matrix from the identification of the system. The corrections to be applied are the product of the inverse of this matrix by the vector to be minimized, in practice the deviations of the ray centroids on the XCCD, as a function of the slit position. Fig 4 shows the focal plane distributions in both directions and corresponding slope errors when the bending routine has been finished. The precision of the slope wavefront error as analyzed in the focal plane by the XCCD camera is less than 20 nm rms, and strongly depends on the vibration level of the set up. After integration, this information provides an error map of the mirror surfaces with respect to the perfect ellipse. The figuring metrology precision has been measured to be 25-nm rms, an information which will be used with deterministic correction tools as the ion beam-milling machine [8]. From its principle, we believe that the accuracy of this metrology is close to its precision and is therefore able to help manufacture diffraction limited quality surfaces.

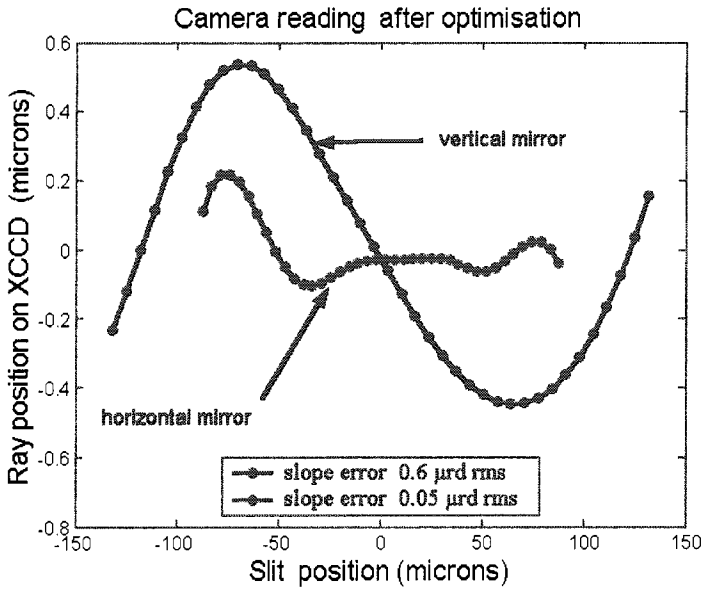

Fig 4 Focus plane distribution as a function of the slit position for both mirrors . The exact local slope is deduced from these curves by dividing each ray position by the distance between the CCD and the ray position at the mirror level.

6.2 Prediction of the performances

Both substrates have been provided by Wave Precision (Moorpark, CA). When the vertical slit is reduced to 200 microns, the vertical slope error reduces to 0.16 microradian rms A spot size of 0.18X0.25 micron (HXV) FWHM is modeled by the ray-tracing program from a 0.2X0.25 mm aperture. The 170-mm mirror is a constant width type because an optimized trapezoidal shaped substrate of sufficient quality was not available at the time of the experiment. The X-ray measured slope and the long trace profiler (LTP) slope errors are very close to the third order polynomial slope predicted by the difference between the ellipse and the bent constant width beam model. This means that the polishing and clamping errors are not predominant when the mirror is illuminated over more than its central 75 mm.

6.6 Vibrations/ drift influence

In order to be consistent with the predicted performances, the depth of focus is Δs = +/- 50 µm, the angle drift tolerance $\Delta\theta$ =1.5 µradian, and the relative radius drift is $\Delta R/R$ = 0.5 %. The vibration level of the vertically focusing mirror has to be less than 0.5 microradian PV, which proved to be unachievable with the set up of this experiment.

6.7 Spot size measurements

The results of the micromirror scans in both directions are shown in Fig. 5. The fact that the 0.6-micron FWHM does not reduce with the aperture size, how small it becomes, and that the quality of the surface as measured by both LTP and

Xray metrology predicts a smaller spot, strongly suggests a limitation by the vibration level of the environment. The irradiance gain was estimated at G=3.5 10^5

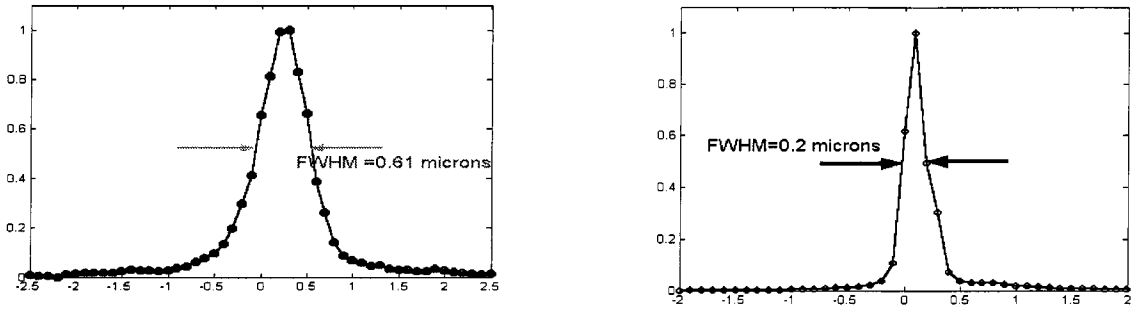

Vertical scan Horizontal scan

Fig. 5 Vertical and horizontal FWHM sizes of the microspot measured with a micromirror, equivalent to a slit width of 0.15 μm.

6.8 Projection microscopy images

The focused spot can be used to perform point by point imaging by scanning the sample in the two transverse directions through the focal spot (see § 6.9). It can also act as a new source to obtain radiographs magnified by projection. Such a full field approach is very promising to overcome the limited spatial resolution (about one micron) due to the X-ray detector in the absence of magnification. If the sample is set downstream of the focus at a distance z_1 and a two-dimensional detector is set at a much larger sample detector distance z_2, a magnified image is obtained with magnification

$$M = \frac{z_1 + z_2}{z_1}$$

The image will be sensitive to the phase modulation introduced by the sample through propagation. It can be shown that a radiograph obtained in such a projection microscope with spherical wave illumination is a magnified version of the image under plane wave illumination and an equivalent sample detector distance (or defocusing distance) D given by

$$D = \frac{z_1 . z_2}{z_1 + z_2}$$

To obtain a large magnification, the sample is set close to the focus ($z_1 << z_2$) and the defocusing distance D will be approximately equal to the focus sample distance ($D = z_1$). The field of views (illuminated portion of the sample) being limited by the angular acceptance of the mirror system, it is not possible to set the sample too close to the focus. In the present imaging experiment the angular acceptance was set to about 2.2 mrad and 0.8 mrad in respectively the horizontal and vertical direction.

For the experiment, performed at an X-ray energy of 20.5 keV (λ = 0.6 Å), we used a detector system based on a 5 μm thick Gadox converter screen coupled through light optics to a cooled Fast REad-out LOw Noise camera developed at the ESRF. The effective pixel size at the level of the scintillator of the detector is 4.9 μm. the exposure time of the images was 60 seconds, but visible contrast could be observed in a few seconds.

Fig. 6a shows the image of a gold test grating with varying period obtained at an X-ray energy of 20.5 keV (λ = 0.6 Å). The focus sample distance was set to 22 mm, whereas the focus detector distance was fixed for all experiments and equal to 3.14 m. The image was corrected for non-uniform illumination by a flat field procedure, i.e. it was divided by an image obtained without sample and the CCD dark current was subtracted from all images. The image is magnified but appears partially blurred. The origin of this contrast reduction was traced back to vibrations caused by the air conditioning system of the building. Fig.6b shows the same object with the cooling system turned off resulting in a very significant gain of contrast. This confirms the idea that mechanical vibrations presently limit the mirror system.

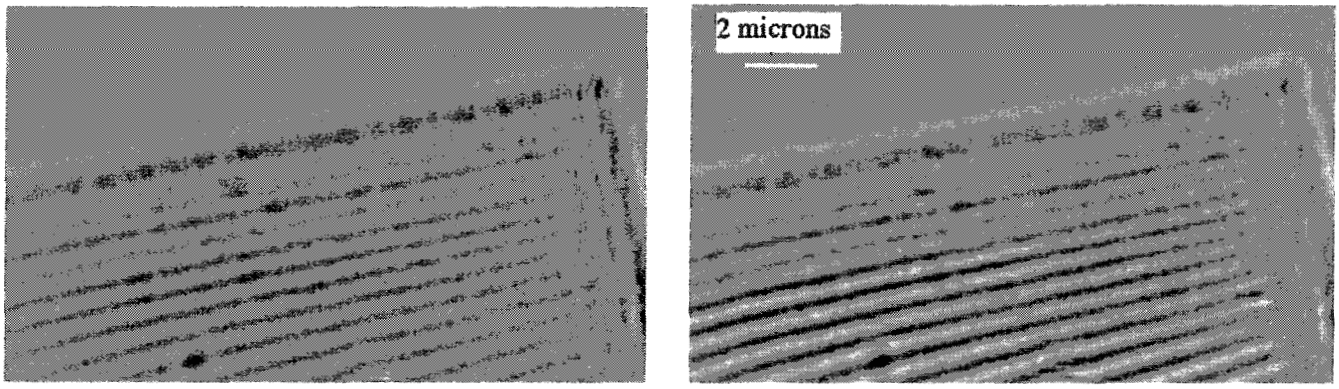

(a) (b)

Fig. 6 Projection image of a gold grating with variable period, (a) with active air conditioning system and (b) without mechanical vibrations due to the cooling system. The X-ray energy was 20.5 keV. The spot focused by the KB system was used as an effective point source. The focus sample distance z_1 was set to 22 mm and the focus detector distance to 3.14 m, resulting in a magnification M of 145.

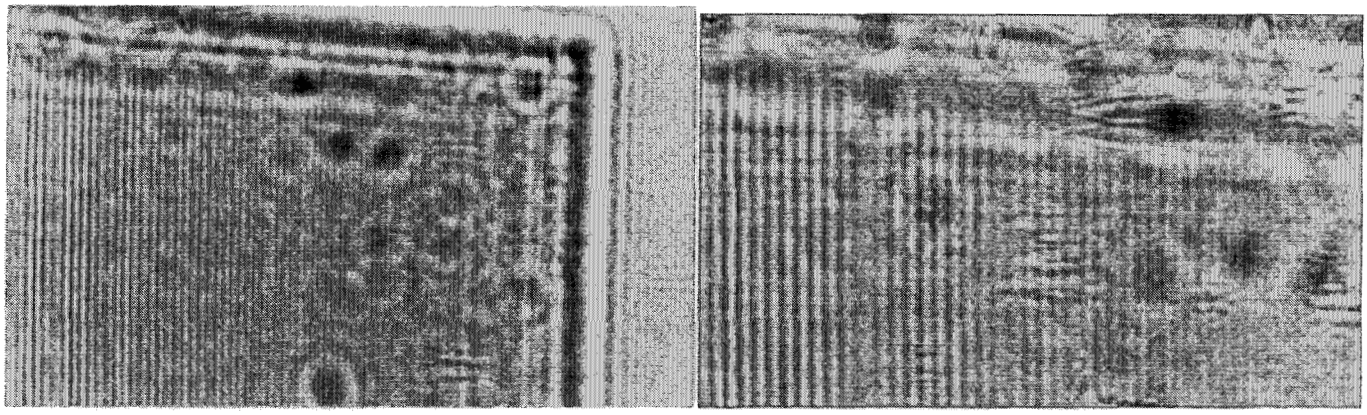

(a) (b)

Fig. 7 Projection images of the gold grating with the lines set vertical. (a) M = 145, z_1 = 22 mm (b) Magnified portion of (a) with M = 268, z_1 = 12 mm The smallest period that can be detected is about 300 nm (line width 150 nm).

The visibility of the finest lines gives an idea of the spatial resolution in the image (actually a Fresnel diffraction pattern). Figure a and b were obtained with the lines of the grating set vertically. These images measure the horizontal resolution and the quality of the horizontal focus. The finest period that can be distinguished clearly is of the order of 300 nm (line width 150 nm). This number corresponds well to the observed spot size. The magnification M was 145 and 268 in figure a and b respectively, with defocus distances 22 mm and 12 mm.

Figure 8 shows a large region of the grating with variable period under identical conditions as in figures 6 and 7 (M = 145, D = 22mm). The lines appear with very high contrast in some regions of the image whereas the contrast seems to disappear in specific regions. This is a direct consequence of the strong dependence of Fresnel diffraction on the size of the object or the spatial frequency. A phase object with period a will show no contrast for distances such that $D = (p/2).\ a2\ /\ \lambda$ with p an arbitrary even number, whereas the contrast is maximum for p odd. To obtain information on all length scales in the object and to retrieve the phase introduced by the object it is therefore necessary to combine images with different defocus [7].

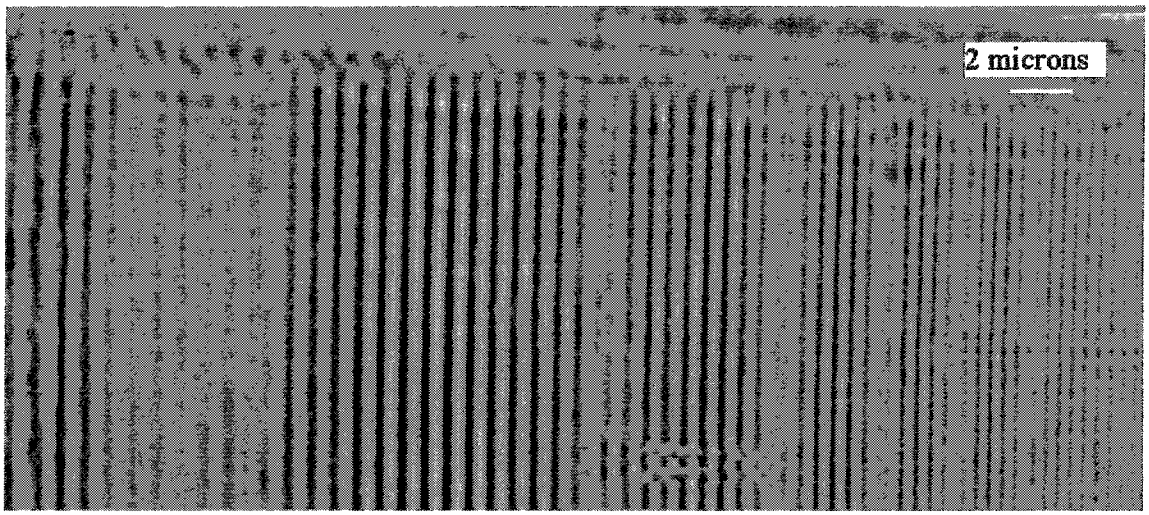

Fig. 8 Projection image of a gold grating with variable period. The lines appear with very high contrast in some regions of the image whereas the contrast seems to disappear in other regions corresponding to different spatial frequencies. Magnification M = 145, z_1 = 22 mm, pixel size: 34 nm.

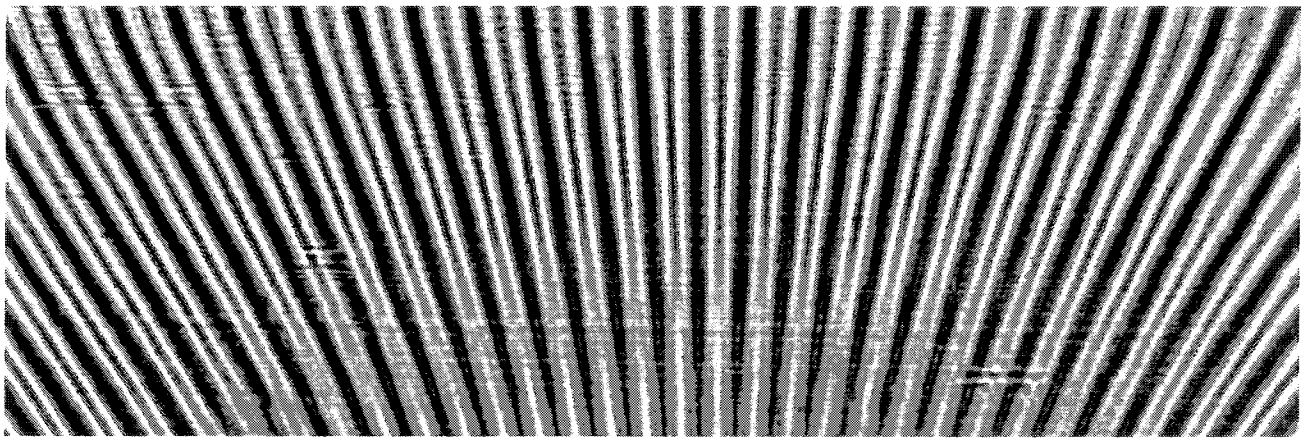

Fig. 9 A star image displaying contrast inversions as a function of spatial frequency

6.9 Microfluorescence

When the sample is set in the plane of the focus and scanned in the transverse directions it is possible to map any signal coming from the sample, such as the fluorescence yield. A nickel bi-crystal wetted along its grain boundary by liquid bismuth was imaged at room temperature using this modality. The fluorescence signal corresponding to the L-edges of bismuth was collected. The grain boundary was set vertical and scanned horizontally with the submicron spot to characterize the thickness of the bismuth wetting layer and its variations in the vertical direction along the grain boundary. The thickness decreases continuously from a macroscopic, several micron thick layer to a submicron width. In the region shown in figure 10 the bismuth signal suddenly disappear. The two profiles shown in Fig. 11, perpendicular to the layer immediately before its apparent end indicate a width of respectively 700 nm and 560 nm. The bismuth fluorescence signal is undetectable along a portion of the grain boundary and reappears at the other end of the bi-crystal plate. This sudden variation in the thickness of the wetting layer suggests a change in the wetting mechanism at this level.

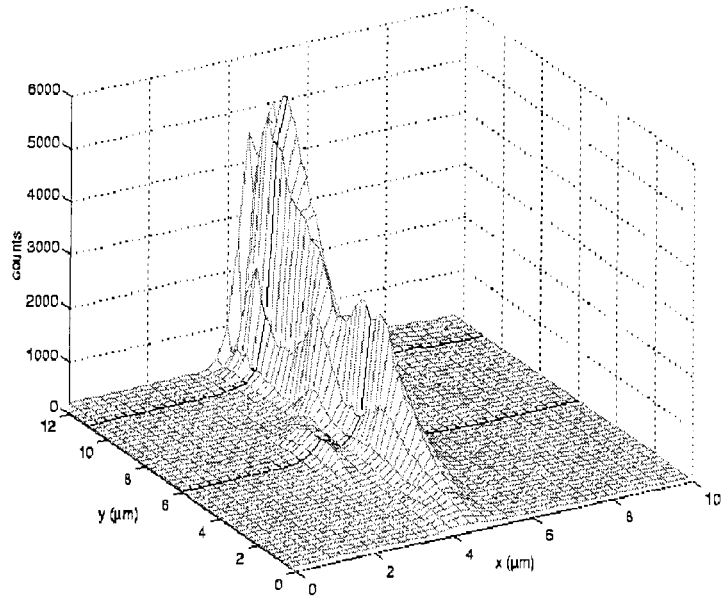

Fig 10 Bismuth L-edge microfluorescence scanning image obtained with a spot of 0.2X0.6 µm FWHM. It shows the wetting of a nickel bi-crystal by liquid bismuth.

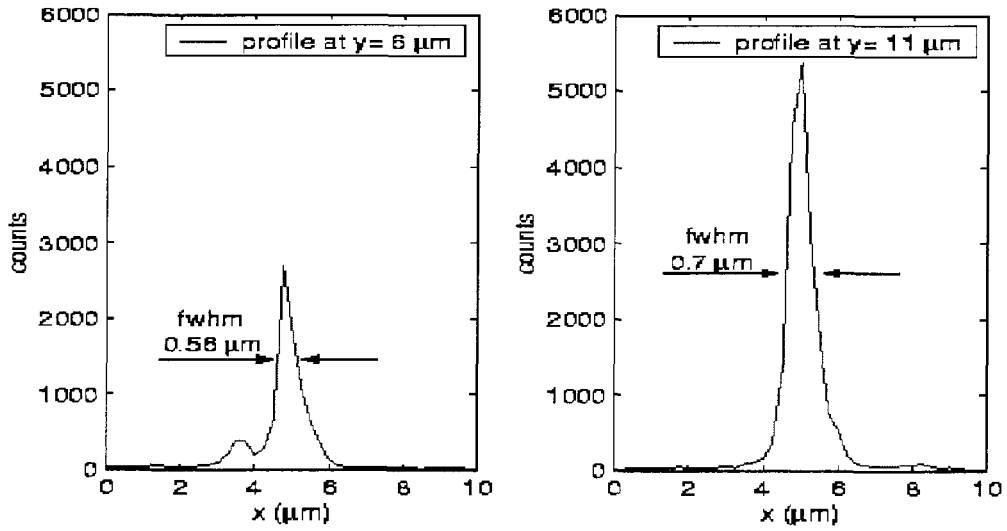

Fig. 11 Two profiles before the bismuth layer thickness ends

6.10 Future efforts and perspectives

Mastering the vibration and drift levels of the supporting structure is a first priority. As an example, a KB I system with 3 meters working distance has been permanently installed on ID13 on a concrete block with locked manual prealignment fixtures. The vibration level was measured as 0.5 and 0.2 microradian PV in vertical and horizontal directions respectively, a level which would probably improve significantly the results obtained in the ID 19 experiment. We plan to improve the mirror surface quality according to the in situ Xray metrology with the help of the ESRF ion beam-milling machine[8]. The status of these technologies allows to predict a diffraction limited performance of the mirrors (i.e. 0.8 nanometers rms figure error) in a near to medium term future. Keeping this quality at tunable angles, with a bent surface, clamped or glued, with corresponding tolerances on width and thickness uniformity, remains a challenge. A tight thermal management might be necessary for angular drift control. If these tasks are mastered, a source limited and diffraction limited performance in horizontal and vertical directions respectively. It could become possible on a long

beamline as ID19, with a FWHM spot size of 92 and 65 nanometers. The use of multilayers is very promising to increase the acceptance of the system, especially at higher energies, but the needed surface quality is then even tighter.

7. CONCLUSION

We achieved an improved performance of Kirkpatrick-Baez optics for the focusing of hard x-rays by obtaining a focal spot size of 200 x 600 nm^2 and a gain of 3.5 x 10^5 at an x-ray energy of 19 KeV. First in-line holographic images obtained showed very high quality. Several systems with different mirror sizes have been designed and built. The ultimate goal, namely a diffraction-limited spot size below 100 nm, is coming closer, but is not yet attained. We trust that by using shape corrected mirrors of a figure error on the nm level obtained with ion beam milling and still some mechanical improvements the ultimate goal will be reached in the near future. In parallel to this mechanical system, we developed a CCD camera based technique to speed up and easy the alignment. We also set up a precise method for measuring very small spot sizes by applying pseudo-slits based on specular reflection from narrow mirror stripes that permit nanometric resolution and replace the knife-edge scanning technique. Finally very high mechanical stability must be ensured by an optimized, integrated design.

8. ACKNOWLEDGEMENTS

We thank M. Panitz, Institute for X-ray physics, University of Goettingen, Germany and C.David , Laboratory for Micro- and Nanotechnology, Paul Scherrer Institute, Switzerland, for providing the nanostructures used in projection microscopy images.

9. REFERENCES

1. J.H. Underwood, A.C. Thompson, J.B. Kortright, K.C. Chapman and D. Lunt, *Focusing x-rays to a 1 μm spot using elastically bent, graded multilayer coated mirrors*, Proc. SRI'95, Rev. Sci. Instrum. **67**, CD-ROM (1995).

2. H.A. Padmore *et al., Submicron white beam focusing using elliptically bent mirrors*, Synchrotron Radiation News **10**, No. 6, 18-25, (1997).

3. P. Eng, M. Newville, M. Rivers and S.R. Sutton, *Dynamically figured Kirkpatrick-Baez x-ray microfocusing optics*, SPIE Proc. **3449**, 145 (1998)

4. L. Zhang, O. Hignette, E. Ziegler and A.K. Freund, *Design optimisation of a flexural hinge-based bender for x-ray optics*, J. Synchrotron Radiation **5,** 804-807 (1998

5. M. Howells *et al., Theory and practice of elliptically bent X-ray mirrors*, Opt. Eng. **39**(10), 2748-2762 (2000).

6. J.Susini, *Design parameters for hard X-ray mirrors* Opt Eng. **34** (2), 361-376 (1995)

7 P.Cloetens, w. ludwig, j. baruchel, d. van dyck, j. van landuyt, j.-p. guigay, m. schlenker ,*Holotomography: quantitative phase tomography with micrometer resolution using hard synchrotron radiation X-rays,* Appl. Phys. Lett. **75**, 2912-2914 (1999).

8. O. Hignette, J.C. Peffen, A. Rommeveaux, V. Alvaro and A.K. Freund, *Towards the preparation of optical surfaces preserving the coherence of hard x-ray beams*, these proceedings.

9. O. Hignette, A.K. Freund and E. Chinchio, *Incoherent X-ray mirror surface metrology*, SPIE Proceedings **3152**, 188-199 (1997).

10. O. Hignette and P. Cloetens, *Metrology and manufacturing of coherence preserving synchrotron X-ray optics*, Proc. 2nd Euspen International Conference, Torino, Italy, May 27, 2001.